Thermal diffusivity monitoring during the stages of formation of core–shell structures of SiO$_2$@Au

Angel Netzahual-Lopantzi[1] · José Francisco Sánchez-Ramírez[2] · Gloria Saab-Rincón[3] · José Luis Jiménez-Pérez[1]

Abstract

The thermal and optical properties in the formation of gold nanoshells on SiO$_2$ were studied by thermal lens (TL) and absorption spectroscopy. The formation of SiO$_2$@Au particles was realized in four stages: First, SiO$_2$ spheres were synthesized using the Stöber method. Later the attachment of amino groups and the adsorption of hydroxide gold nanoparticles on surface of silicon dioxide were realized. Finally, the growth of gold shell was obtained. The UV–Vis spectrum of SiO$_2$@Au nanostructures showed an absorption band in the near-infrared region around of 740 nm associated with the presence of a gold shell on the dielectric platform. Transmission electron microscopy and scanning electron microscopy confirmed the formation of well-defined gold nanoshell on SiO$_2$ spheres. Silicon dioxide nanospheres with an average size of 293 nm and Au-nanoshell with thicknesses of ~14 nm were obtained. The high crystalline quality of Au-nanoshell was demonstrated by X-ray diffraction. The thermal diffusivity during the different steps of formation of the gold nanoshell was studied using absorption spectroscopy and the mode-mismatched TL. A redshift of absorption band optic was observed by UV–Vis, and a very significant increase in the thermal diffusivity as the Au shell was completed.

Keywords Thermal diffusivity · Thermal lens spectroscopy · SiO$_2$@Au nanoparticles

1 Introduction

In recent years, interest on SiO$_2$@Au core–shell nanostructures has increased as a result of the changes they have in their optical and thermal properties compared to their homogeneous counterparts. The gold nanoshells or core–shell (SiO$_2$@Au) structures consist of a silicon dioxide sphere surrounded by a nanometric layer of gold, i.e., metallodielectric colloids. Gold nanoshells are materials that have

a highly tunable surface plasmon resonance (SPR) and are observed as an absorption band located from the visible region to near-infrared in the electromagnetic spectrum; this optical property is dependent on the relative thickness of the SiO$_2$ core and its metallic shell, i.e., core/shell diameter ratio [1], when the ratio value increases, the absorption band can be displaced to longer wavelength. In infrared region (800 nm), the water (solvent in biological systems) and hemoglobin have minimal absorption [2]. Therefore, Au nanoshells with intense absorption at near-infrared wavelengths can be used in thermal assays in vitro, in vivo and other applications in biomedical areas, in addition to its compatibility with biological systems [3].

While gold nanoshells have been prepared using different types of templates, for example, polystyrene (PS) microspheres with average size of 700 nm were used for the synthesis of Au shell with 10 nm of thickness [4]. Gold shells on ~200 nm liposomes soybean lecithin were prepared by Wu et al. [5]. Ag nanoparticles (~40 nm) served as platform to grow a thin gold nanoshell (~14 nm) reported by Grabowska-Jadach et al. [6]. SiO$_2$ spheres also serve as template for the synthesis of gold nanoshells, the key factor in the growth of metallic shell is the replacement of silanol

✉ Angel Netzahual-Lopantzi
lopantzi_@hotmail.com

1 Unidad Profesional Interdisciplinaria en Ingeniería y Tecnologías Avanzadas-Instituto Politécnico Nacional, Av. Instituto Politécnico Nacional No. 2580, Col. Barrio la Laguna Ticomán, Del. Gustavo A. Madero, C.P. 07340 Ciudad de Mexico, D.F., Mexico

2 Centro de Investigación en Biotecnología Aplicada-Instituto Politécnico Nacional, Ex-Hacienda San Juan Molino Carretera Estatal Tecuexcomac-Tepetitla Km 1.5, C.P. 90700 Tlaxcala, Mexico

3 Departamento de Ingeniería Celular y Biocatalisis, Instituto de Biotecnología, Universidad Nacional Autónoma de México, 62250 Cuernavaca, Morelos, Mexico

(Si–OH) groups with organic ligands such as amino groups NH_2, and the amine groups form bonds with gold species [7] The PS, liposomes and Ag templates mentioned above have some disadvantages, because of the evaporation process under nitrogen, and storage is required for a long time. SiO_2 nanospheres with well-defined size and monodispersity can be quickly obtained using the Stöber method.

The preparation of silicon dioxide spheres decorated with Au particles is necessary for the synthesis of nanoshells, and a common route is the synthesis of SiO_2 and gold nanoparticles in separate solutions, but using the citrate reduction method, the reaction is very slow [8]; SiO_2 and Au solutions are aged for several weeks, and then, the colloidal solutions are mixed to grow a thin metallic shell on dielectric platform [9]. Kadnpal *et at.* [8] reported the synthesis of $SiO_2@$ Au structures using SiO_2 spheres of 260 nm as template, gold shell with thickness of ~ 20 nm was obtained by SEM micrographs, and the UV–Vis spectrum revealed an absorption band around 529 nm. Silica spheres (140 nm) decorated with gold nanoparticles (3-5 nm) were mixed with $HAuCl_4$ (0.04 mM), hydroxylamine hydrochloride ($NH_2OH.HCl$) and polyvinylpyrrolidone were added, the solution was sonicated, gold nanoshells (thickness = 25 nm) were obtained, and an absorption band around 700 nm was recorded using UV–Vis spectroscopy [7]. Although the aforementioned methods are efficient to synthesize core–shell structures, it is necessary to perform more than one procedure for its synthesis, becoming tedious methods.

The core–shell structures can be synthesized quickly and efficiently using the one-step method. This method involves the deposition of $Au(OH)_3$ particles on SiO_2 spheres, without the need for prior synthesis of colloidal gold, and each $Au(OH)_3$ particle is a nucleation site to form a complete thin shell on SiO_2 [10]. The growth kinetics of gold nanoshell has been monitored by microscopy and spectroscopy techniques. The formation of monomers, dimers and trimmers of gold nanoshells was reported using TEM microscopy [11]. Bisacetonitrile gold (I) complex was deposited on silica particles (65-430 nm), and the reduction in Au° and the formation of thin shell on dielectric platform using ascorbic acid were revealed by proton nuclear magnetic resonance (^{1}H NMR) spectra [12]. Oldenburg et al. [1] studied the synthesis kinetics of gold nanoshells using UV-Vis spectroscopy, a redshift of absorbance peak (520 to 800 nm) was reported. On the other hand, thermal lens (TL) technique has been used for study nanofluids, for example, nanofluids containing gold nanoparticle. Au nanoparticles (~ 5 nm) were dispersed in water at a concentration of 3.18 mg/ml, and thermal diffusivity of 16.8×10^{-4} cm^2/s was recorded using photoflash technique [13]. However, to our knowledge, TL has not been used to study the formation of gold nanoshells. In this work, the thermal properties of water-based gold nanoshell are characterized in their different formation stages on SiO_2 nanospheres using the LT. Thermal diffusivity measurements of the SiO_2 nanospheres are also obtained. The formation of $SiO_2@Au$ nanostructured is confirmed using TEM, SEM, EDS, X-Ray, XPS and UV–Vis spectroscopy. The gold nanoshells formation was monitored using UV–Vis and thermal lens spectroscopy.

2 Methodology

2.1 Materials

The reagents used for the preparation of the $SiO_2@Au$ structures were: tetraethyl orthosilicate (TEOS, 99%), ammonium hydroxide (NH_4OH, 28-30% as ammonia NH_3), (3-aminopropyl) triethoxysilane (APTES), tetrachloroauric acid ($HAuCl_4.3H_2O$, 99.99%), sodium borohydride ($NaBH_4$ 98%), sodium citrate dihydrate ($OHC (COONa) (CH_2 COONa)_2 2H_2O$, 99%) and potassium carbonate (K_2CO_3). All were acquired from Sigma-Aldrich. Methanol (CH_3OH 99%), ethanol (C_2H_5OH 99%), sodium hydroxide (NaOH 99%) were obtained from J.T. Baker. Deionized water was employed for preparing the solutions (Millipore system with resistivity 18.2 MΩ cm)

2.2 Preparation SiO_2

It was possible to prepare spherical structures of monodisperse SiO_2 with an average size of 293 nm using the Stöber method reported elsewhere [14]. Briefly, 6.5 ml of ammonium hydroxide, 2.3 ml of water and 0.5 ml of TEOS were mixed in a volumetric flask to 60 ml with ethanol. 0.075 g of SiO_2 spheres clean of pollutants was functionalized with APTES (a bifunctional molecule) at concentration of 0.012 mol/l to obtain amino groups on the surface of SiO_2 spheres.

2.3 Preparation seed solution

The one-step method was used for the synthesis of gold nanoshells [10]. The method involves in the preparation of SiO_2 spheres with $Au(OH)_3$ particles on surface, and this new structure is called *seed* precursor. Briefly, a solution of gold hydroxide containing 3 ml of sodium hydroxide (0.1 mol/l) with 10 ml of $HAuCl_4$ (6.35 mol/l) was prepared. Then, 10 ml of gold hydroxide was mixed with 0.075 g of SiO_2 amino-functionalized, the mixture was heated at 70 °C with vigorous stirred during 30 min, and according to theory, the process carried out is for homogeneous deposition of gold hydroxide $Au(OH)_3^-$ on the surface of the SiO_2 spheres [10]. The product was washed by centrifugation (8000 rpm for 60 min) at least five times; finally, the sample

was dissolved in 100 ml of water. The colloidal solution was called *seed solution*.

2.4 Synthesis of nanoshells

The theory dictates that the each gold hydroxide nanoparticle $Au(OH)_3$ deposited on SiO_2 spheres acts as nucleation site, and each nanoparticle grows in size due to the presence of more gold molecular precursor until its eventual coalescence to form a complete and continuous gold shell around the template SiO_2. For achieve this, 1.5 ml of $HAuCl_4$ (25 mmol/l) solution was poured into a flask with 100 ml of deionized water, 60 mg of K_2CO_3 was added and was stirred overnight, the mix reached a pH $\approx$ 10.8 containing gold hydroxide $[Au(OH)_4]^-$, and the solution was called *k-gold.*

Different volumetric ratios of seed/k-gold were mixed (1:1, 1:3, 1:5, 1:9 and 1:20) with a constant volume of k-gold of 7.5 ml, sodium borohydride (6.6 mmol/l) and sodium citrate (10 mmol/l) were added, and the solution was stirred during 30 min. The resulting colloidal solution was washed (by centrifugation) and dried at 60 °C for 12 h until powders were obtained.

2.5 Characterization

The formation and characterization of gold nanoshells were carried out using spectroscopy and microscopy techniques: For scanning electron microscopy characterization (SEM/EDS, model JEOL JSM IT300 with Energy-Dispersive X-Ray Spectroscopy), the samples in water were deposited on aluminum. For UV–Vis spectroscopy (spectrophotometer Genesys 10S, Thermo Scientific), the measurements were taken on samples dispersed in water. For transmission electron microscopy (TEM, model JEOL JEM 1010), each of the colloidal samples was deposited on a copper grid (covered with a FORMVAR film) until the solvent was evaporated at room temperature. Rigaku Smartlab diffractometer in the Bragg–Brentano configuration was used for measurements of X-ray diffraction (XRD), the samples were analyzed in powder using the CuK_α radiation ($\lambda = 1.5418$ Å), and the diffractometer was operated at a scan rate of 0.02°/s over a 2θ range of 10-90°. The XPS spectra were obtained from X-ray Photoelectron spectrometer Thermo Scientific K-Alpha, and a monochromated AlKα excitation line at 1487 eV was used. To obtain the measurements, the samples were dropped on aluminum until solvent evaporated, and the spectrometer was calibrated using the C1s peak around 284.6 eV arising from the adventitious hydrocarbon.

2.6 Thermal lens

Thermal diffusivity was determined by thermal lens spectroscopy. This technique involves the incidence of an excitation laser with a Gaussian profile on the sample causing the absorbed energy transformed into heat. In this case, a temperature gradient is established, and a change of refractive index. When a second probe laser is passed in the sample, an effect of focusing or defocusing of the light beam is caused, and this phenomenon produced is called thermal lens [14, 15].

The mode-mismatched dual-beam experimental arrangement of thermal lens spectrometry is observed in Fig. 1, the sample was exposed to an excitation laser (Ar$^+$Xe), where it is generate a local temperature increase, and also, the probe beam (He–Ne) passes through the sample propagating until photodiode.

The photodiode is used to detect intensity dependence of the probe beam transmitted or propagated to far field in center of the beam $I(t)$, to detector is [16]:

$$I(t) = I(0) \left[1 - \frac{\theta}{2} \tan^{-1} \left(\frac{2mV}{[(1 + 2m)^2 + V^2] \frac{t_c}{2t} + 1 + 2m + V^2} \right) \right]^2$$

(1)

Fig. 1 Thermal lens setup. The excitation and probe beams in mode-mismatched. PD is photodiode, and *l*o is the length of the quartz cell
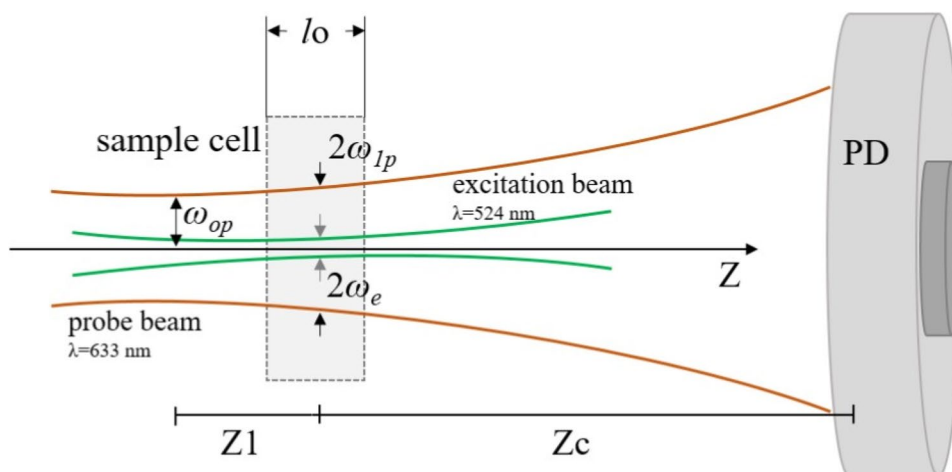
where

$$V = \frac{Z_1}{Z_c}, m = \left(\frac{\omega_p}{\omega_e}\right)^2, t_c = \frac{\omega_{e^2}}{4D}, \theta = -\frac{P_e A_e l_o}{k\lambda_p}\left(\frac{dn}{dT}\right), \quad (2)$$

where $I(t)$ is the time dependent of probe beam to detector, $I(0)$ is the initial value of $I(t)$ for t zero, Zc (12.89 cm) is the confocal distance of probe beam, $Z1$(8 cm) is the distance of the sample the probe beam waist, ω_e (4.8×10^{-3} cm) and ω_p (1.81×10^{-2} cm) are the spot size of excitation laser and probe beam, respectively, to the sample, t_c is the characteristic time constant, λ_e refers to the wavelength of the excitation beam, λ_p is the wavelength of probe beam, D and k are the diffusivity and conductivity thermal of sample, P_e is the power of excitation beam, A_e is the optical absorption coefficient to wavelength of the excitation laser, l_o (1 cm) is the sample thickness, and dn/dT is the refractive index dependent temperature of sample. For measurements of thermal diffusivity, metallodielectric colloids were dispersed in deionized water, to ensure dispersion correct of particles, and the samples were subjected in ultrasound for 10 min.

3 Results and discussion

SiO$_2$ structures were synthesized using the Stöber method [17], and the SiO$_2$ particles were used as templates for the growth of the gold shells. The formation of SiO$_2$ structures was investigated by SEM microscopy. A well-defined spherical structure was observed in SEM micrograph (as shown in Fig. 2a), and the average size was approximately 293 nm published elsewhere [14]. Inset of Fig. 1a corresponds to EDS analysis by mapping, and the results revealed the exclusive presence of oxygen and silicon similar results to

early reports [18]. Gold nanoshells were synthesized using the one-step method (with slight modifications) proposed by Kah and coworkers [10]. The methodology used in this work is schematized in Fig. 2b. Stage 1 consisted of the preparation of SiO$_2$ particles using TEOS as a molecular precursor. As the second stage, the dielectric platform was amino-functionalized using APTES. Au(OH)$_3$ nanoparticles were deposited on SiO$_2$-NH$_2$ structures in third place. Finally, as the last stage, stage 4 consisted of the growth of a thin shell on dielectric platform using SiO$_2$-Au(OH)$_3$ mixed with k-gold solution. The SiO$_2$ spheres were amino-functionalized because Au is a metal with little affinity to SiO$_2$; for this reason, amino groups were anchored on SiO$_2$ because the gold is high affinity to NH$_2$ groups [10].

Each stage during the formation of core–shell structures was characterized by UV–Vis spectroscopy. The spectra of SiO$_2$ spheres (a), SiO$_2$ amino-functionalized (b), SiO$_2$-Au(OH)$_3$ (c) and gold nanoshells or SiO$_2$@Au (d) are shown in Fig. 3. Before and after functionalization of SiO$_2$ spheres, no absorption band was recorded in the visible or near-infrared region, and the effect in the seed solution (i.e., SiO$_2$ decorated with Au(OH)$_3$ nanoparticles) was also observed. The core–shell SiO$_2$@Au structures were synthesized using a volumetric ratio 1:5 of seed and K-gold solution, respectively, a broad spectrum with a maximum of absorption at 740 nm was observed (spectrum d in Fig. 3), and similar to other reports [8], as the inset shows, the characteristic solution was obtained.

The growth of gold nanoshell on SiO$_2$ platform was monitored by UV–Vis spectroscopy. For this reason, several samples were mixed at different volumetric ratios of seed solution and k-gold (1:1, 1:3, 1:5, 1:9, and 1:20, respectively). Figure 4 shows UV–Vis spectra a), b), c), d) and e) of samples synthesized according to the increase
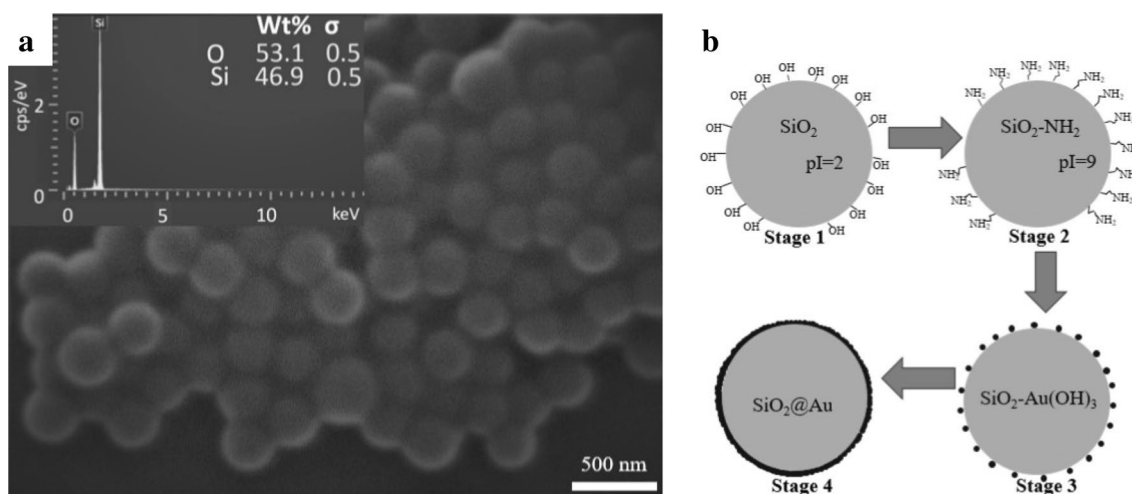

Fig. 2 **a** SEM micrograph of SiO$_2$ spheres synthesized with 6.5 ml of ammonium hydroxide, **b** schematic representation of each stage during synthesis of gold nanoshells. *Inset* of 1a): EDS spectrum of SiO$_2$ spheres
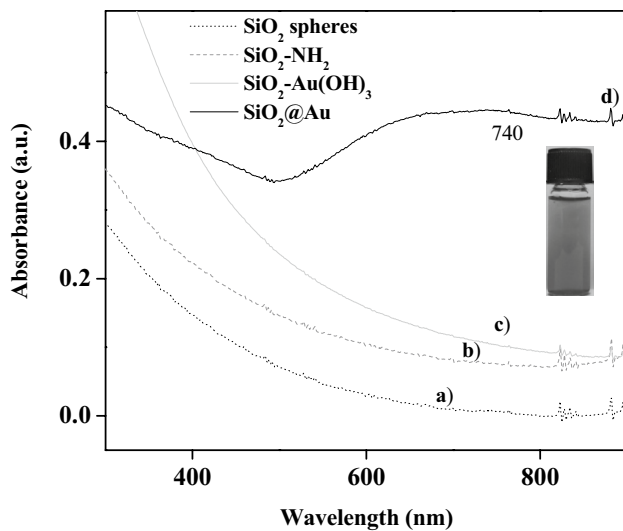
Fig. 3 UV–Vis spectra of **a** SiO$_2$ spheres, **b** SiO$_2$ functionalized with NH$_2$, **c** SiO$_2$ with Au(OH)$_3$ nanoparticles, **d** SiO$_2$@Au core–shell nanoparticles. The *inset* shows the colloid obtained
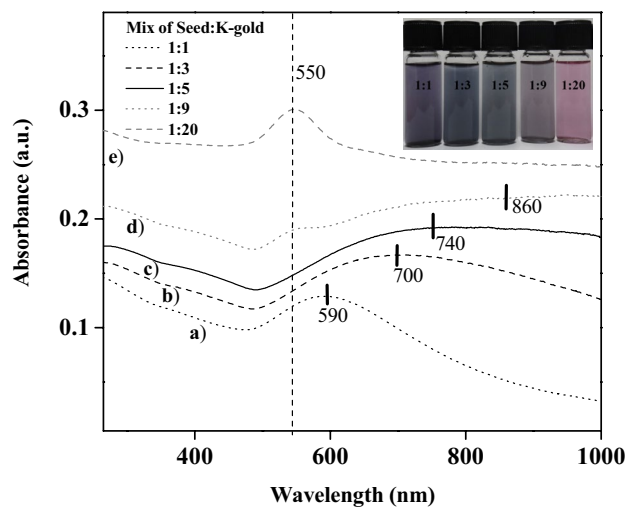
Fig. 4 UV–Vis spectra of SiO$_2$@Au core–shell nanoparticles synthesized with volume ratio at **a** 1:1, **b** 1:3, **c** 1:5, **d** 1:9 and **e** normalized spectrum of sample with 1:20 of seed/K-gold, respectively. The *inset* shows the colloids solutions obtained

in the k-gold solution. The results showed an increase in the redshift of the absorption band according to volume k-gold, with a maximum absorption around 590, 700 and 740 nm for samples containing volumetric ratio of seed/k-gold at 1:1, 1:3 and 1:5, respectively. The redshift effect in the peak optical absorption is related as coalescence of the gold layer progresses according to Oldenburg et al. [1]. The authors suggested that each gold hydroxide nanoparticle Au(OH)$_3$ grows in size until its eventual coalescence (junction between particles) forms a complete and continuous gold shell around the template SiO$_2$. Here, samples

with a ratio 1:1 recorded a spectrum similar to that gold colloid solution, and this means that the k-gold solution was not enough to synthesize a gold shell. Increasing the ratio of gold molecular precursor in samples 1:3, 1:5 and 1:9, a displacement to long wavelengths of absorption band was observed. But in the sample 1:9, two absorption peaks were recorded around 860 and 550 nm, and the band in visible region observed is related to the synthesis of gold nanoparticles outside the nanoshells, the presence of aggregates or incomplete shells [11]. Increasing a volumetric a ratio of seed/k-gold at 1:20, only absorption band around 550 nm was recorded, and also, the red color in the solution was observed as shown in the inset of Fig. 4, so the synthesis of gold nanoparticles was confirmed. According to UV–Vis spectra, a complete gold shell was synthesized with a volumetric ratio of 1:5 (seed/k-gold), because it has the major redshift with one absorption band around 740 nm.

The formation of gold nanoshells was revealed through TEM, SEM microscopy and EDS spectroscopy. Figure 5a shows micrograph TEM of structures core–shell, spherical particles are clearly observed, and a roughness at the edge of each gold shell was observed, because a gold coverage on the SiO$_2$ sphere was completed. The average size particle after shell synthesis was estimated, and a diameter ~ 322 nm was recorded, as shown in the inset of Fig. 4a. The shell thickness ~ 14 nm was calculated. In this work, the diameter ratio of core–shell was ~ 22:1, and values above were reported by Kandpal et al. [8] with ratio of ~ 13:1. Micrographs SEM revealed spherical shape for core–shell structures synthesized using one-step method. Elemental mapping was recorded by EDS, and the inset in Fig. 5b shows the silicon, oxygen and gold without any other contaminant element [19].

Figure 6 shows the typical XRD peaks of the as-synthesized gold nanoshells, the crystalline structure of the sample is well defined by the five sharp peaks at 2θ values of 38.3° (111), 44.4° (200), 64.7° (220), 77.4° (311) and 81.8° (222) related for the face-cubic-centered structure of gold, according to The CCDC/FIZ Karlsruhe assigned deposition service number was CCDC 1881812 [14]. The shell thickness D was determined from the Debye–Scherer's equation, $D = \frac{0.9\lambda}{\beta * \cos\theta}$ where $\lambda = 0.15414$ nm is the wavelength of the incident radiation, β is the full width at half maximum (FWHM) of the XRD peak, and θ is the Bragg angle. D value = 13.5 nm of thickness gold shell was calculated. With these results, the synthesis of polycrystalline shell deposited on SiO$_2$ spheres was confirmed. The SiO$_2$ spheres had no detectable sharp diffraction peaks corresponding to any crystalline phase, data not shown.

The elemental oxidation state of SiO$_2$@Au core–shell structures was investigated by XPS spectroscopy. Figure 7

Fig. 5 **a** TEM and **b** SEM micrographs of SiO$_2$@Au nanoshells. *Insets*: 5a) size distribution histogram, 5b): EDS spectrum of core–shell structures
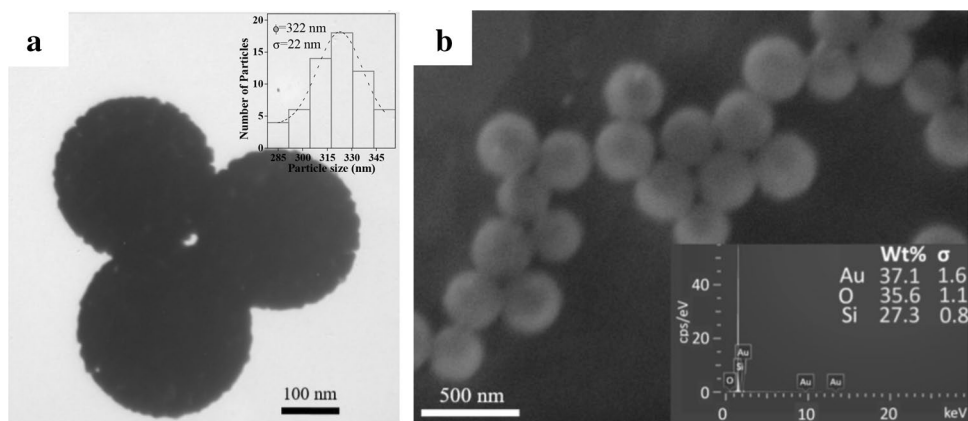
Fig. 6 XRD pattern of gold nanoshell synthesized using one-step method
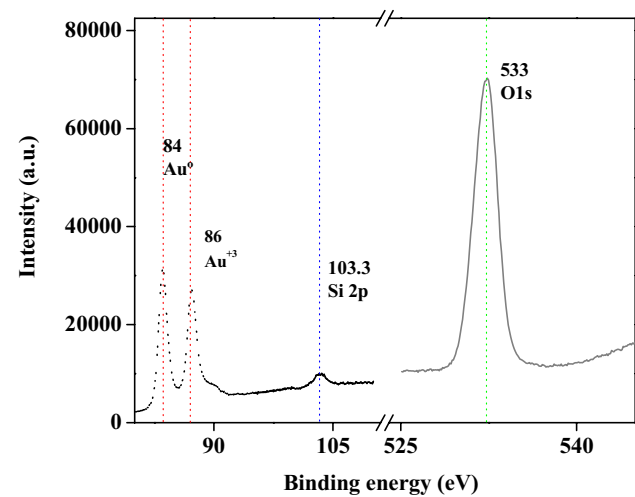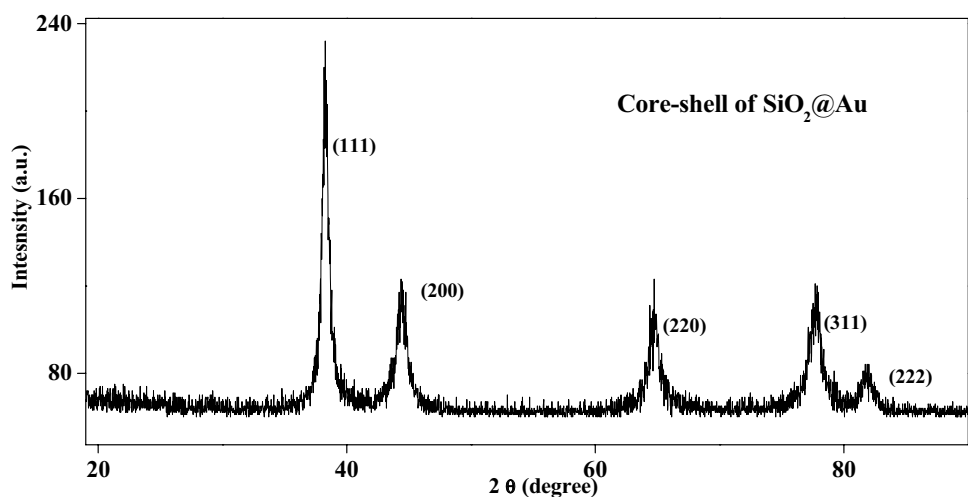

Fig. 7 High-resolution XPS spectra of Auº, Au^{+3}, Si 2p and O1s states for SiO$_2$@Au nanostructures

shows the XPS spectra of the sample. For Au 4f, two peaks are localized around 84 and 86 eV related to Auº y Au^{+3}, respectively, evidencing the presence of gold in a metallic state. These spectra were similar to Sun et al. [20]. The Si 2p exhibits a peak to 103.3 eV that corresponds to lattice silicon [21]. Finally, a clearly defined peak was observed to 533 eV related to lattice oxygen O1s [22]. These results confirmed the formation of core–shell structures of SiO$_2$@Au.

Each stage during synthesis of gold nanoshell was monitored by thermal lens spectroscopy; thus, thermal diffusivity was obtained. The colloids were dried to obtain powder. The samples were dissolved in water to different concentrations from 0.1 to 0.7 mg/ml. A typical spectra of the TL signal as a function of time are shown in Fig. 8. The signal intensity decreased with time, the open circles represent the obtained experimental data, and the solid line represents the best fitting of Eq. (1) to the experimental data.

The method Stöber was used for synthesis of SiO$_2$ particles. The method involves the hydrolysis and condensation of tetraethyl orthosilicate (TEOS), and the products obtained
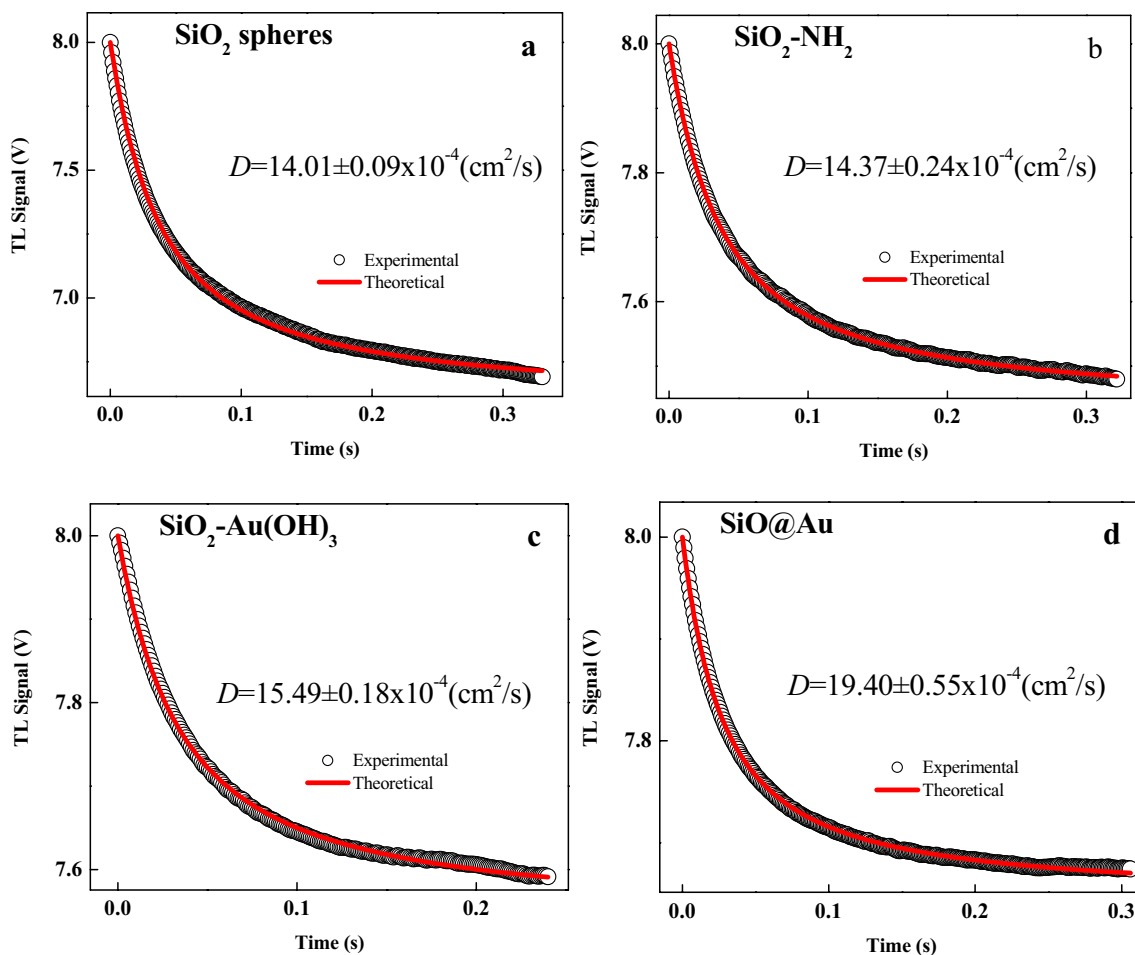
Fig. 8 Thermal lens signal for **a** stage 1, **b** stage 2, **c** stage 3 and **d** stage 4, during the synthesis of gold nanoshell using one-step method. The TL signal corresponds to samples at concentrations of 0.1/ml

are Si–OH and Si–O–Si respectively. The growth in silica particle size depends on the amount of Si–O–Si monomer in a synthesis solution [23, 24]. The concentrations of molecular precursors used in this work allowed obtained SiO_2 spheres with average size of 293 nm. SiO_2 spheres were characterized by thermal lens spectroscopy. The parameters θ and t_c were obtained fitting the thermal lens signal as function of time and thermal diffusivity was calculated using Eq. (2). The results for t_c a range from $4.28 \pm 0.02 \times 10^{-3}$ s to $3.50 \pm 0.09 \times 10^{-3}$ s and for θ, between $22.07 \pm 0.62 \times 10^{-2}$ and $5.37 \pm 0.63 \times 10^{-2}$ were recorded (as shown in Table 1). For SiO_2 spheres with concentrations of 0.1-0.7 mg/ml, thermal diffusivity values were between $14.01 \pm 0.09 \times 10^{-4}$ and $17.06 \pm 0.57 \times 10^{-4}$ cm^2/s, and these results were similar to early reports [25].

In the stage 2 (Fig. 2b) during synthesis of gold nanoshells, the SiO_2 spheres were amino-functionalized using 3-aminopropyl-triethoxysilane (APTES), i.e., SiO_2-NH_2 structures (Fig. 2b). Table 2 shows the values of characteristic time (t_c) range from $4.17 \pm 0.07 \times 10^{-3}$ s

Table 1 Parameters obtained by thermal lens spectroscopy of SiO_2 spheres dispersed in deionized water

SiO_2 spheres				
Sample	Concentration	D	t_c	θ
	mg/ml	D (10^{-4} cm^2)	s (10^{-3})	10^{-2}
a	0.1	14.01 ± 0.09	4.28 ± 0.02	22.07 ± 0.62
b	0.2	14.39 ± 0.14	4.16 ± 0.04	19.17 ± 1.24
c	0.3	15.03 ± 0.15	3.99 ± 0.04	12.03 ± 2.68
d	0.4	15.47 ± 0.13	3.87 ± 0.03	5.81 ± 0.34
e	0.5	16.01 ± 0.21	3.74 ± 0.04	5.96 ± 0.31
f	0.6	16.58 ± 0.36	3.62 ± 0.08	5.37 ± 0.63
g	0.7	17.06 ± 0.57	3.50 ± 0.09	6.31 ± 0.24

to $3.00 \pm 0.03 \times 10^{-3}$ s and of θ, from $8.74 \pm 0.24 \times 10^{-2}$ to $4.74 \pm 0.31 \times 10^{-2}$ for SiO_2 amino-functionalized. The thermal diffusivity values between $14.37 \pm 0.24 \times 10^{-4}$ cm^2/s and 20.02 ± 0.23^{-4} cm^2/s were recorded, and the thermal values were higher than in the SiO_2 spheres at all concentrations.

Table 2 Parameters obtained by thermal lens spectroscopy of SiO$_2$-NH$_2$ structures dispersed in deionized water

SiO$_2$ amino-functionalized				
Sample	Concentration	D	t_c	θ
	mg/ml	D (10^{-4} cm^2/s)	s (10^{-3})	10^{-2}
a	0.1	14.37 ± 0.24	4.17 ± 0.07	8.74 ± 0.24
b	0.2	14.94 ± 0.25	4.02 ± 0.06	7.85 ± 0.22
c	0.3	16.03 ± 0.26	3.73 ± 0.06	8.55 ± 0.25
d	0.4	17.07 ± 0.20	3.51 ± 0.04	7.28 ± 0.20
e	0.5	17.98 ± 0.21	3.33 ± 0.03	5.96 ± 0.29
f	0.6	18.86 ± 0.16	3.18 ± 0.02	4.74 ± 0.31
g	0.7	20.02 ± 0.23	3.00 ± 0.03	5.06 ± 0.22

The grafting of APTES on the silica nanoparticles caused a change in isoelectric point (pI) of silica particles from 2 to 9 [10], and this is because amine groups have a pKa = 9. In this work, an increase in thermal diffusivity was recorded in SiO$_2$-NH$_2$ structures, although the mechanism of increase in thermal parameter is unknown, similar results are reported by Wondu and coworkers [26], the authors used the APTES as filler and coupling agent in polymers to form thermal interface materials, using laser flash analysis (LFA), transient method thermal conductivity was estimated, and an increase in thermal conductivity was recorded due to the presence of APTES [26, 27].

In the stage 3, the SiO$_2$-NH$_2$ structures and a solution of gold hydroxide (Au(OH)$_3$Cl$^-$) were mixed under pH = 8 [28]. The electrostatic bond between cation (NH$_2^+$) and anion (Au(OH)$^-_3$) was performed; as consequence, SiO$_2$ decorated with Au(OH)$_3$ nanoparticles was obtained according to Kah et al. [10]. In this work, the SiO$_2$-Au(OH)$_3$ structures (Fig. 2b) were called seed solution. The SiO$_2$-Au(OH)$_3$ structures to different concentrations (0.1-0.7 mg/ml) were measured by thermal lens spectroscopy. The values for the characteristic time (t_c) range from $3.87 \pm 0.04 \times 10^{-3}$ s to $2.68 \pm 0.02 \times 10^{-3}$ s and for θ, from $6.97 \pm 0.22 \times 10^{-2}$ to

$3.82 \pm 0.09 \times 10^{-2}$, as shown in Table 3. Thermal diffusivity values were between $15.49 \pm 0.18 \times 10^{-4}$ cm^2/s and $22.34 \pm 0.24 \times 10^{-4}$ cm^2/s, and these thermal values of SiO$_2$-Au(OH)$_3$ were higher than SiO$_2$-NH$_2$ structures and SiO$_2$ spheres. The thermal increased is related to presence metallic species on the silica particles, because metallic increased thermal diffusivity of dielectric platforms [29].

Finally, in stage 4, the seed solution containing SiO$_2$-Au(OH)$_3$ was mixed with a solution of gold hydroxide (Au(OH)$_4$)$^-$ at a volumetric ration of 1:5, respectively, and then, sodium borohydride was added; this allowed the growth of a thin metallic layer on SiO$_2$ spheres. Different concentrations of core–shell of SiO$_2$@Au were dispersed in water and characterized by thermal lens spectroscopy. Table 4 shows the parameter θ with values from $5.43 \pm 0.24 \times 10^{-2}$ to $0.29 \pm 0.15 \times 10^{-2}$. For t_c values between $4.28 \pm 0.02 \times 10^{-3}$ s and $3.50 \pm 0.09 \times 10^{-3}$ s, a drastic decrease in t_c was recorded in the last stage; therefore, thermal diffusivity values were major than early stages. The core–shell structures at 0.1-0.7 mg/ml recorded thermal diffusivity values from $19.4 \pm 0.55 \times 10^{-4}$ cm^2/s to $52.4 \pm 1.38 \times 10^{-4}$ cm^2/s, respectively. The minimum concentration of SiO$_2$@Au structures provided thermal diffusivity of $19.4 \pm 0.55 \times 10^{-4}$ cm^2/s that is higher than other structures like silver nanowires [30] with 17.75×10^{-4} cm^2/s of thermal diffusion rate.

An increase in thermal diffusivity was recorded as progress stages formation of SiO$_2$@Au nanostructures. In the stage 1, the silica particles naked recorded thermal diffusivity values low (as shown in Fig. 9), because the SiO$_2$ is high reflective [31] and large percentage of the incident light is reflected. In the second stage, the grafting of APTES on the silica nanoparticles caused an increase in thermal parameter. Later, in the stage 3, the deposition of Au(OH)$_3$ particles on SiO$_2$-NH$_2$ favored a thermal improvement, and this is due to the presence of gold although in oxidation state [29]. Up to here, the sensibility of thermal lens spectroscopy is high because it was

Table 3 Parameters obtained by thermal lens spectroscopy of SiO$_2$ decorated with Au(OH)$_3$ nanoparticles in deionized water

SiO$_2$-Au(OH)$_3$				
Sample	Concentration	D	t_c	θ
	mg/ml	D (10^{-4} cm^2/s)	s (10^{-3})	10^{-2}
a	0.1	15.49 ± 0.18	3.87 ± 0.04	6.97 ± 0.22
b	0.2	16.44 ± 0.17	3.65 ± 0.03	5.44 ± 0.34
c	0.3	17.52 ± 0.16	3.42 ± 0.03	6.21 ± 0.16
d	0.4	18.52 ± 0.24	3.24 ± 0.04	5.97 ± 0.23
e	0.5	19.46 ± 0.27	3.08 ± 0.04	5.25 ± 0.15
f	0.6	21.04 ± 0.40	2.86 ± 0.04	4.75 ± 0.15
g	0.7	22.34 ± 0.24	2.68 ± 0.02	3.82 ± 0.09

Table 4 Parameters obtained by thermal lens spectroscopy of core–shell SiO$_2$@Au nanoparticles dispersed in 1 ml of deionized water

Core–shell structure of SiO$_2$@Au				
Sample	Concentration	D	t_c	θ
	mg/ml	D (10^{-4} cm^2/s)	s (10^{-3})	10^{-2}
a	0.1	19.40 ± 0.55	3.09 ± 0.08	5.43 ± 0.24
b	0.2	26.50 ± 0.41	2.26 ± 0.03	4.43 ± 0.12
c	0.3	31.60 ± 0.51	1.89 ± 0.03	2.97 ± 0.05
d	0.4	36.90 ± 0.76	1.62 ± 0.03	1.47 ± 0.03
e	0.5	40.30 ± 1.11	1.48 ± 0.04	1.55 ± 0.08
f	0.6	45.70 ± 1.42	1.31 ± 0.04	0.52 ± 0.03
g	0.7	52.40 ± 1.38	1.14 ± 0.03	0.29 ± 0.15
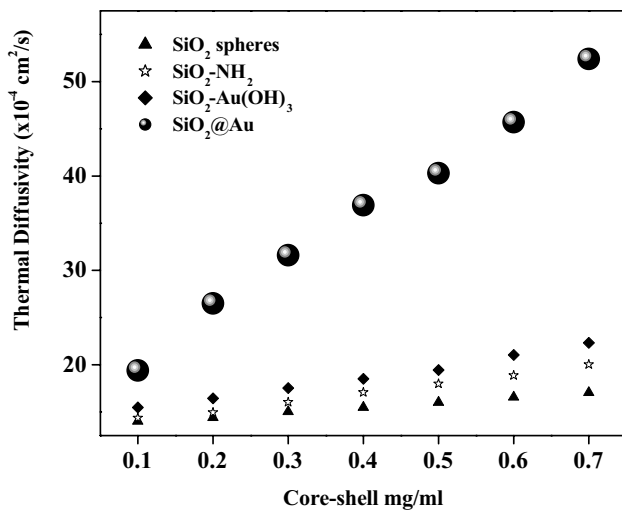
Fig. 9 Thermal diffusivity of metallodielectric samples as a function of concentration

possible to record an increase in thermal diffusivity as there is a progress in chemical modification on dielectric platform (according to scheme in Fig. 2b). In the stage 4, the greatest increase in thermal diffusivity was recorded, and this is because gold nanoshell was completed (evidenced in the UV–Vis spectrum c) in Fig. 4). The thermal effect in the last stage could be explained below. The gold is characterized by has high rate of conversion of light to heat. The energy transformation process begins with electron–electron interactions leading hot electrons, after the electron passes the energy to the phonon by electron–phonon interactions (taking place in less than femtoseconds), resulting in a hot lattice with a temperature rise. The lattice cools off by passing its heat to the surrounding medium via phonon–phonon relaxation [32], and this process leads to the heat up of the surrounding medium (water in this case). Now, Huang and coworkers [33] reported that in Au nanospheres (SPR $\lambda = 560$ nm), the electron–phonon relaxation time is about 3.1 picoseconds, but for gold nanoparticles with absorption band to 860 nm, the relaxation time is faster around 1.6 picoseconds. The authors also mentioned that nanoparticles with tuning in the infrared region had 10% energy more than spherical. Here, the $SiO_2@Au$ structures have an absorption band in the near-infrared region ($= 740$ nm); therefore, the increase in thermal diffusivity could be explained by the rapid electron–phonon relaxation. On the other hand, all samples in each stage during synthesis of gold nanoshell showed an increase in thermal diffusivity as concentrations of colloids were increases, and this dependency can be attributed to the volumetric increase in the nanoparticles that decreases the specific heat of the water; consequently, the thermal diffusivity of the colloidal suspension increases [34].

In this work, gold shells thickness ~ 14 nm (evidenced by TEM and XRD) was grown on SiO_2 spheres to form $SiO_2@$ Au nanostructures. With this, thin metallic layer provided thermal diffusivity up to $52.4 \pm 1.38 \times 10^{-4}$ cm²/s, which is higher than Au@Ag structures reported by Gutierrez-Fuentes et al. [35]. The authors reported thermal values of $23.39 \pm 0.41 \times 10^{-4}$ cm²/s in Ag shells of ~ 8.5 nm. The thermal difference may be due to the fact that as the thickness of the metal shell increases, the heat transfer also increases, according to the theoretical results reported by Nikbakht in 2018 [36]. Finally, the use of $SiO_2@Au$ nanostructures provides two main advantages, optical absorption at wavelengths near-infrared [2] where the water has minimal absorption coefficient. Second, the high conversion of light to heat provides the heat transfer to surrounding medium (evidenced by thermal lens spectroscopy). Therefore, $SiO_2@$ Au nanostructures can be used in thermal assays in vitro, in vivo and other applications in biomedical areas, in addition to its compatibility with biological systems.

4 Conclusion

In summary, the core–shell structures of $SiO_2@Au$ were prepared using one-step method efficiently. The metallodielectric particles recorded an absorption band around 740 nm shown by UV–Vis spectroscopy. Gold shells (~ 14 nm) were successfully grown on SiO_2 spheres, confirmed by TEM, SEM/EDS, XRD and XPS. An increase in thermal diffusivity was recorded as the Au shell was completed, i.e., stage 1 (SiO_2 spheres), stage 2 (SiO_2–NH_2), stage 3 (SiO_2-Au(OH)$_3$) and stage 4 ($SiO_2@Au$). The thermal results suggest that thermal lens spectroscopy can be good technique to study growth kinetics of metallodielectric colloids with high sensibility. The thermal diffusivity values of $SiO_2@Au$ structures recorded by thermal lens spectroscopy were higher than SiO_2 spheres naked. Therefore, core–shell structures tuning in infrared region and with a high light-to-heat conversion rate can be used in thermal therapy, in solar cell or SERS effect. Finally, this work can serve as a basis for further studies in photothermal assays against cancer cells.

References

1. S.J. Oldenburg, R.D. Averitt, S.L. Westcott, N.J. Halas, Nanoengineering of optical resonances. Chem. Phys. Lett. **288**, 243–247 (1998). https://doi.org/10.1016/S0009-2614(98)00277-2
2. R. Weissleder, A clearer vision for in vivo imaging. Nature **19**, 316–317 (2001). https://doi.org/10.1038/86684

3. L. Tang, L. Liu, H.B. Elwing, Complement activation and inflammation triggered by model biomaterial surfaces. J. Biomed. Mater. Res. **41**, 333–340 (1998). https://doi.org/10.1002/(SICI)1097-4636(199808)41:2%3c333:AID-JBM19%3e3.0.CO;2-L

4. T. Ji, V.G. Lirtsman, Y. Avny, D. Davidov, Preparation, characterization, and application of au-shell/polystyrene beads and Au-Shell/magnetic beads. Adv. Mater. **13**, 1253–1256 (2001). https://doi.org/10.1002/1521-4095(200108)13:16%3c1253:aid-adma1253%3e3.0.co;2-t

5. W. Wu, C. Yu, M. Chu, A gold nanoshell with silica inner shell synthesized using liposome templates for doxorubicin loading and near-infrared photothermal therapy. Int. J. Nanomed. **6**, 807–813 (2011). https://doi.org/10.2147/IJN.S16701

6. I. Grabowska-Jadach, D. Kalinowska, M. Drozd, M. Pietrzak, Synthesis, characterization and application of plasmonic hollow gold nanoshells in a photothermal therapy New particles for theranostics. Biomed. Farmacother. **111**, 1147–1155 (2019). https://doi.org/10.1016/j.biopha.2019.01.037

7. K. Wang, Y. Wang, C. Wang, X. Jia, J. Li, R. Xiao, S. Wang, Facile synthesis of high-performance SiO_2@Au core–shell nanoparticles with high SERS activity. RSC Adv. **8**, 30825–30831 (2018). https://doi.org/10.1039/c8ra05213a

8. D. Kandpal, S. Kalele, S. Kulkarni, Synthesis and characterization of silica–gold core-shell (SiO2@Au) nanoparticles. Pramana J. Phys. **69**, 277–283 (2007). https://doi.org/10.1007/s12043-007-0128-z

9. J. Choma, A. Dziura, D. Jamiola, P. Nyga, M. Jaroniec, Preparation and properties of silica-gold core-shell particles. Colloids Surf. A **373**, 167–171 (2011). https://doi.org/10.1016/j.colsurfa.2010.10.046

10. J.C.Y. Kah, N. Phonthammachai, R.C.Y. Wang, J. Song, T. White, S. Mhaisalkar, I. Ahmadb, C. Shepparda, M. Olivo, Synthesis of gold nanoshells based on the deposition-precipitation process. Gold Bull. **41**, 23–36 (2008). https://doi.org/10.1007/BF03215620

11. V.A. Khanadeev, B.N. Khlebtsov, N.G. Khlebtsov, Optical properties of gold nanoshells on monodisperse silica cores: experiment and simulations. J. Quant. Spectrosc. Radiat. Transf. **187**, 1–9 (2017). https://doi.org/10.1016/j.jqsrt.2016.09.004

12. M.D. English, E.R. Waclawik, A novel method for the synthesis of monodisperse gold-coated silica nanoparticles. J. Nanopart. Res. **14**, 1–10 (2012). https://doi.org/10.1007/s11051-011-0650-2

13. S. Soltaninejad, M.S. Husin, A.R. Sadrolhosseini, R. Zamiri, A. Zakaria, M.M. Moksin, E. Gharibshahi, Thermal diffusivity measurement of Au nanofluids of very low concentration by using photoflash technique. Measurements **46**, 4321–4327 (2013). https://doi.org/10.1016/j.measurement.2013.07.043

14. A. Netzahual-Lopantzi, J.F. Sánchez-Ramírez, J.L. Jiménez-Pérez, D. Cornejo-Monroy, G. López-Gamboa, Z.N. Correa-Pacheco, Study of the thermal diffusivity of nanofluids containing SiO_2 decorated with Au nanoparticles by thermal lens spectroscopy. Appl. Phys. A **125**, 588 (2019). https://doi.org/10.1007/s00339-019-2891-3

15. J.L. Luna-Sánchez, J.L. Jiménez-Pérez, R. Carbajal-Valdez, G. López-Gamboa, M. Perez-Gonzalez, Z.N. Correa-Pacheco, Green synthesis of silver nanoparticles using Jalapeno Chili extract and thermal lens study of acrylic resin nanocomposites. Thermochim. Acta **678**, 178314 (2019). https://doi.org/10.1016/j.tca.2019.178314

16. J. Shen, R. Lowe, R.D. Snook, A model for cw laser induced mode-mismatched dual-beam thermal lens spectrometry. Chem. Phys. **165**, 385–396 (1992). https://doi.org/10.1016/0301-0104(92)87053-C

17. W. Stöber, A. Fink, Controlled Growth of monodisperse Silica Spheres in the Micron Size Range. J. Colloid Interface Sci. **26**, 62–69 (1968). https://doi.org/10.1016/0021-9797(68)90272-5

18. Q. Guo, D. Huang, X. Kou, W. Cao, L. Li, L. Ge, L. Jiangong, Synthesis of disperse amorphous SiO_2 nanoparticles via sol-gel. Ceram. Int. **43**, 92–196 (2017). https://doi.org/10.1016/j.ceramint.2016.09.133

19. Y. An, G. Zhu, W. Bi, L. Lu, C. Feng, Z. Xu, W. Zhang, Highly sensitive electrochemical immunoassay integrated with polymeric nanocomposites and enhanced SiO_2@Au core-shell nanobioprobes for SirT1 determination. Anal. Chim. Acta **966**, 54–61 (2017). https://doi.org/10.1016/j.aca.2017.02.011

20. L. Sun, L. Jiang, S. Peng, Y. Zheng, X. Sun, H. Su, C. Qi, Preparation of Au catalysis supported on core-shell SiO2/polypyrrole composites with high catalytic performances in the reduction of 4-nitrophenol. Synth. Met. **248**, 20–26 (2019). https://doi.org/10.1016/j.synthmet.2018.12.024

21. R. Zhang, Structural and optical properties of grey and porous SiO_2 nanoparticles. Physica B **533**, 23–25 (2019). https://doi.org/10.1016/j.physb.2018.10.027

22. G. Xu, X. Shen, Fabrication of SiO2 nanoparticles incorporated coating onto titanium substrates by the micro arc oxidation to improve the wear resistance. Surf. Coat. Technol. **364**, 180–186 (2019). https://doi.org/10.1016/j.surfcoat.2019.01.069

23. I.A. Rhaman, P. Vejayakumaran, C.S. Sipaut, J. Ismail, M.A. Bakar, R.K.C. Adnan, An optimized sol-gel synthesis of stable primary equivalent silica particles. Colloids Surf. A **294**, 102–110 (2007). https://doi.org/10.1016/j.colsurfa.2006.08.001

24. E. Vega-López, U. Morales-Muñoz, El Proceso Stöber: Principios y Actualidad 1ª Parte 9, 19–30 (2016). http://quimica.ugto.mx/index.php/nyt/article/view/Nyt%209-3

25. J.L. Jiménez-Pérez, J.F. Sánchez-Ramírez, D. Cornejo-Monroy, R. Gutiérrez-Fuentes, J.A. Pescador-Rojas, A. Cruz-Orea, C. Jacinto, Photothermal study of two different nanofluids containing SiO_2 and TiO_2 semiconductor nanoparticles. Int. J. Thermophys. **33**, 69–79 (2012). https://doi.org/10.1007/s10765-011-1139-z

26. E. Wondu, Z. Lule, J. Kim, Thermal Conductivity and Mechanical Properties of Thermoplastic Polyurethane-/Silane-Modified Al_2O_3 Composite Fabricated via Melt Compounding. Polymers **11**, 1–12 (2019). https://doi.org/10.3390/polym11071103

27. D.S. Muratov, D.V. Kuznetsov, I.A. Il'inykh, I.N. Burmistrov, I.N. Mazov, Thermal conductivity of polypropylene composites filled with silane-modified hexagonal BN. Compos. Sci. Technol. **111**, 40–43 (2015). https://doi.org/10.1016/j.compscitech.2015.03.003

28. S. Ivanova, V. Pitchon, C. Petit, H. Herschbach, A.V. Dorsselaer, E. Leize, Preparation of alumina supported gold catalysts: gold complexes genesis, identification and speciation by mass spectrometry. Appl. Catal. A **26**, 203–210 (2006). https://doi.org/10.1016/j.apcata.2005.10.018

29. M. Hari, S.A. Joseph, S. Mathew, B. Nithyaja, V.P.N. Nampoori, P. Radhakrishnan, Thermal diffusivity of nanofluids composed of rod-shaped silver nanoparticles. Int. J. Therm. Sci. **64**, 188–194 (2013). https://doi.org/10.1016/j.ijthermalsci.2012.08.011

30. R. Carbajal-Valdez, A. Rodríguez-Juárez, J.L. Jiménez-Pérez, J.F. Sánchez-Ramírez, A. Cruz-Orea, Z.N. Correa-Pacheco, M. Macías, J.L. Luna-Sánchez, Experimental investigation on thermal properties of Ag nanowire nanofluids at low concentrations. Thermochim. Acta **671**, 83–88 (2019). https://doi.org/10.1016/j.tca.2018.11.015

31. A. Netzahual-Lopantzi, J.F. Sánchez-Ramírez, J.L. Jiménez-Pérez, Comparative study of the thermal diffusivity of SiO_2–Au nanoparticles in water base. Appl. Phys. A **126**, 588 (2020). https://doi.org/10.1007/s00339-020-3346-6

32. X. Huang, M.A. El-Sayed, Gold nanoparticles: optical properties and implementations in cancer diagnosis and photothermal therapy. J Adv Res **1**, 13–28 (2010). https://doi.org/10.1016/j.jare.2010.02.002

33. W. Huang, Q. Qian, M.A. El-Sayed, Y. Ding, Z.L. Wang, Effect of the lattice crystallinity on the electron-phonon relaxation rates in

gold nanoparticles. J. Phys. Chem. C **111**, 10751–10757 (2007). https://doi.org/10.1021/jp0738917

34. F.M. Ali, W.M. Yunus, Study of the effect of volume fraction concentration and particle materials on thermal conductivity and thermal diffusivity of nanofluids. Jpn. J. Appl. Phys. **50**, 085201 (2011). https://doi.org/10.1143/JJAP.50.085201

35. R. Gutierrez Fuentes, J.A. Pescador Rojas, J.L. Jimenez-Perez, J.L. Sánchez-Ramírez, A. Cruz-Orea, J.G. Mendoza-Alvarez, Study of thermal diffusivity of nanofluids with bimetallic nanoparticles with Au(core)/Ag(shell) structure. Appl. Surf. Sci. **255**, 781–783 (2008). https://doi.org/10.1016/j.apsusc.2008.07.023

36. M. Nikbankht, Radiative heat transfer between core-shell nanoparticles. J. Quant. Spectrosc. Radiat. Transf. **221**, 164–171 (2018). https://doi.org/10.1016/j.jqsrt.2018.10.005

Publisher's Note Springer Nature remains neutral with regard to jurisdictional claims in published maps and institutional affiliations.